2 μm Raman fiber laser based on a multimaterial chalcogenide microwire

Nurmemet Abdukerim, Lizhu Li, Mohammed El Amraoui, Younès Messaddeq, and Martin Rochette

Citation: Appl. Phys. Lett. **110**, 161103 (2017); doi: 10.1063/1.4980128
View online: http://dx.doi.org/10.1063/1.4980128
View Table of Contents: http://aip.scitation.org/toc/apl/110/16
Published by the American Institute of Physics

2 μm Raman fiber laser based on a multimaterial chalcogenide microwire

Nurmemet Abdukerim,[1,a)] Lizhu Li,[1] Mohammed El Amraoui,[2] Younès Messaddeq,[2] and Martin Rochette[1]
[1]*Department of Electrical and Computer Engineering, McGill University, Montréal H3A 0E9, Canada*
[2]*Center for Optics, Photonics and Lasers (COPL), Laval University, Québec City G1V 0A6, Canada*

(Received 8 February 2017; accepted 2 April 2017; published online 17 April 2017)

We report a Raman fiber laser based on a multimaterial chalcogenide microwire. The microwire structure comprises a core of $As_{38}Se_{62}$, a cladding of $As_{38}S_{62}$, and a coating of poly-methyl methacrylate. The microwire is a robust, high confinement waveguide compatible with the mid-infrared. With the microwire inserted in a ring cavity, Raman laser oscillation at a wavelength of 2.025 μm occurs from synchronous pumping at a wavelength of 1.938 μm. The input peak power required to reach threshold is 4.6 W and the power slope efficiency is 4.5%. Numerical simulations are in good agreement with experimental results and predict chirp-free femtosecond pulses. *Published by AIP Publishing*. [http://dx.doi.org/10.1063/1.4980128]

The Raman gain is of widespread use in laser cavities, especially convenient to generate light at any wavelength for which resonant gain media are not available.[1] In silica fibers, the Raman gain provided by silica has led to Raman fiber lasers.[2] Various forms of continuous wave (CW) and pulsed Raman fiber lasers have been extensively studied.[3–7] Previous studies using the Raman gain in silica fibers mostly focused on the wavelength range of 1.0–1.6 μm for imaging and telecommunications related applications. Targeting emission wavelengths beyond 2 μm for biomedical and chemical sensing applications, Raman fiber lasers have been demonstrated using GeO_2-doped silica fibers but the low Raman gain coefficient combined with high transmission losses of silica leads to high power threshold and low efficiency.[8]

In contrast with silica, chalcogenide glasses have a Raman gain coefficient as high as 900 times that of silica and wide transmission window extending up to 11 μm (As_2S_3) and 16 μm (As_2Se_3) in the mid-infrared.[9–11] These properties bring chalcogenide fibers as excellent candidates for the development of Raman fiber lasers at wavelengths >2 μm. To date, only a few Raman lasers based on chalcogenide fibers have been reported.[12–15] One of them provides the longest wavelength for Raman fiber lasers with 3.77 μm.[12] At the exception of one report showing an all-fiber design,[13] every demonstration relied on free-space optics for pump coupling, making the laser prone to misalignment. The main limitation of the all-fiber concept presented in Ref. 13 is the poly-methyl methacrylate (PMMA) cladding directly applied over the chalcogenide core of the Raman gain medium, impairing transmission in the mid-infrared.

With an aim towards compact and low-power consumption Raman fiber lasers, the access to a large waveguide nonlinearity coefficient of the gain medium is of prime concern. Tapered microwires benefit from a large increase in the waveguide nonlinearity coefficient by hundreds of times with respect to their untapered counterpart.[16,17] However, an unprotected fiber that is tapered down to a diameter in the order of the wavelength results in extreme mechanical fragility. In response to this, high numerical aperture optical fibers with dual-material core-cladding composition (e.g., polymers, As_2Se_3, As_2S_3) have served to build robust microwires.[18–21]

In this letter, we demonstrate an all-fiber Raman laser based on a multimaterial microwire. The microwire consists of a 10 cm long waveguide with a core of $As_{38}Se_{62}$ and a cladding of $As_{38}S_{62}$ coated with PMMA. This microwire provides a strong Raman gain and enables the laser threshold to occur at a peak power as low as 4.6 W. In the microwire, light is confined by mid-infrared compatible materials of a $As_{38}Se_{62}$ core and a $As_{38}S_{62}$ cladding. The microwire is thus a promising candidate for the fabrication of mid-infrared sources that are compact and operate with low-power consumption. Numerical simulations are carried out and predict that the experimentally obtained Raman pulses are linearly chirped and could be compressed to ~500 fs, which is 20 times shorter than pump pulses, showing that the Raman fiber laser is capable of converting picosecond pulses into femtosecond pulses.

The microwire fabrication includes arsenic (As), sulfur (S), and selenium (Se) batched from commercially available elements with purity higher than 99.9999%. The raw materials are placed under vacuum into a sealed silica ampoule and then heated up to 700–800 °C for several tens of hours, quenched in water, and annealed at approximately 170 °C to remove mechanical stress. The core and cladding glass compositions are $As_{38}Se_{62}$ and $As_{38}S_{62}$, respectively. The dual-material $As_{38}Se_{62}/As_{38}S_{62}$ fiber is then drawn by a double crucible method.[22] The dual-chalcogenide fiber is coated with PMMA to result in a multimaterial fiber that enables the fabrication of robust microtapers following the technique detailed in Refs. 18 and 19.

Figure 1(a) presents the geometry of a typical microtaper. It is subdivided into multimaterial fibers on both ends, two intermediate transition sections, and a microwire at the center. Figure 1(b) shows the reflection optical micrograph of a typical multimaterial fiber facet. Both multimaterial fiber ends are butt-coupled to SMF-28 fibers via UV epoxy, resulting in a total insertion loss of 6 dB, including 0.1 dB/cm of

a)Author to whom correspondence should be addressed. Electronic mail: nurmemet.abudukelimu@mail.mcgill.ca

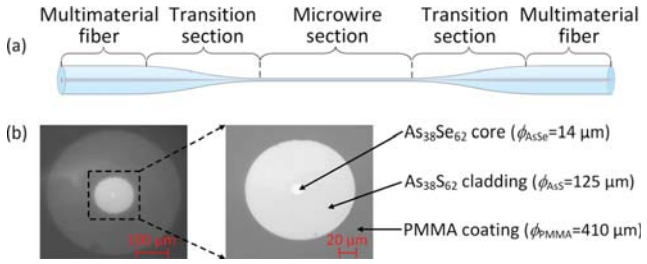

FIG. 1. (a) Microtaper geometry (not to scale). (b) Reflection optical micrograph of a multimaterial fiber facet.

propagation loss, 0.5 dB per interface due to Fresnel reflection loss at chalcogenide-silica interfaces, and the rest is attributed to mode-mismatch and misalignment losses.

The microwire is designed with a core diameter of 0.85 μm to achieve a minimum $A_{\text{eff}} = 0.92\ \mu\text{m}^2$ at the wavelength of 1.938 μm and thus maximize the Raman gain. In the microwire, the fundamental optical mode is tightly confined in the $As_{38}Se_{62}$ core ($n_{\text{AsSe}} = 2.81$) due to large refractive index contrast with respect to the $As_{38}S_{62}$ cladding ($n_{\text{AsS}} = 2.41$). The chosen diameter also leads to chromatic dispersion that is normal with $\beta_2 = 1.67\ \text{ps}^2/\text{m}$, ensuring pure Raman operation without modulation instability. The transmission window of the microwire is only limited by the common transmission windows of $As_{38}Se_{62}$ and $As_{38}S_{62}$, which spans from 1.5 μm up to 11.0 μm, thus making this microwire compatible with mid-infrared applications.

In a first experiment, the Raman gain of the microwire is characterized. Figure 2 shows a schematic of the pump-probe experimental setup. The pump is a thulium-doped mode-locked fiber laser that emits pulses at a wavelength of 1.938 μm, with a full-width at half-maximum (FWHM) duration of 800 fs, and at a repetition rate of 30 MHz. A 100 m long spool of SMF-28 fiber is used to broaden pump pulses before amplification by a thulium-doped fiber amplifier, to avoid the nonlinear effects and pulse distortion in the fiber amplifier. Amplified pulses are subsequently filtered by a 2 nm tunable bandpass filter to eliminate amplified spontaneous emission from the fiber amplifier. The resulting pulses have a FWHM duration of ~10 ps. The probe is a CW fiber laser tunable at wavelengths in between 1.900 μm and 2.036 μm,[23] with a linewidth <0.05 nm, limited by the optical spectrum analyzer (OSA) resolution bandwidth. The pump and the probe are coupled into the microwire by an 80/20 fiber coupler. The peak pump power coupled into the microwire is 2 W, and the CW probe power coupled into the microwire is 0.021 mW independent of the wavelength. A

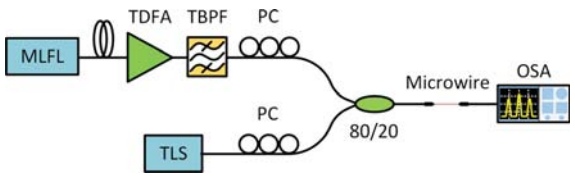

FIG. 2. Schematic of the characterization setup for Raman amplification. MLFL: mode-locked fiber laser; TDFA: thulium-doped fiber amplifier; TBPF: tunable bandpass filter; PC: polarization controller; TLS: tunable laser source; and OSA: optical spectrum analyzer.

polarization controller (PC) is inserted in both the pump and probe arms to align their polarization states in the microwire. Raman gain is measured as a function of probe wavelength from 2.009 μm to 2.036 μm, where the longest wavelength is limited by the tunable range of the probe laser. Output spectra are recorded with an optical spectrum analyzer (OSA, Yokogawa AQ6375), with the resolution bandwidth set to 1 nm.

Figure 3(a) shows the amplified spectra and extracted Raman gain at different probe wavelengths λ_s. Spectral broadening of the probe signal occurs from cross-phase modulation, while it is amplified by Raman gain. The Raman gain at each wavelength is extracted by integrating the amplified spectra without the CW probe and illustrated by red triangles. The contour line shows the Raman gain profile, and dashed part of the contour line is extrapolated to show the expected gain profile at longer wavelengths. The maximum Raman gain of 18.4 dB occurs at 2.030 μm or a wavelength shift of 92 nm, corresponding to a Raman frequency shift of 7.07 THz or 236 cm^{-1}, in agreement with the previously reported values.[9] Figure 3(b) shows the Raman response function of $As_{38}Se_{62}$ extracted from the Lorentzian curve fitting to the measured Raman gain[24]

$$h_R(t) = \frac{\tau_1^2 + \tau_2^2}{\tau_1 \tau_2^2} \exp(-t/\tau_2) \sin(t/\tau_1), \tag{1}$$

where $\tau_1 = 22.5$ fs and $\tau_2 = 342$ fs. Using fractional contribution of delayed Raman response $f_R = 0.1$ and nonlinear refractive index $n_2 = 7.6 \times 10^{-18}\ \text{m}^2/\text{W}$ at 1.94 μm,[25] the inferred peak Raman gain coefficient of $As_{38}Se_{62}$ is $g_R = 2.2 \times 10^{-11}$ m/W at the pump wavelength.

The linearity of the Raman gain is also investigated. Figure 4(a) shows the measured single-pass Raman gain as a function of probe power, whilst the input peak power is kept at 2.1 W. The probe wavelength is set to 2.030 μm. As the coupled probe power is gradually increased up to 0.11 mW, no sign of gain saturation effect is observed. Figure 4(b) shows the Raman gain as a function of coupled peak pump power, whilst the probe power is kept at 0.021 mW at the wavelength of 2.030 μm. The Raman gain linearly increases as the peak pump power is increased without a sign of gain saturation.

Figure 5 shows a schematic of the Raman fiber laser. Amplified and filtered pump pulses are coupled into the Raman laser cavity through a wavelength division multiplexing (WDM) coupler. An 80/20 fiber coupler is used to extract 20% of the power at the output of the cavity. An optical delay line (ODL) serves to adjust the ring cavity length to the pump laser repetition rate. Another PC made of normal dispersion fiber is placed in the cavity to stabilize the polarization state of the laser as well as to compensate the total cavity dispersion. The total cavity dispersion is ~−0.03 ps/nm at the wavelength of 2.025 μm, which is slightly normal dispersion. The total round-trip cavity loss is 12.0 dB, including 1.5 dB for the WDM coupler, 6.0 dB for the microwire, 2.0 dB for the 80/20 coupler plus insertion losses, and 2.5 dB for the ODL. The round-trip cavity loss could be reduced to <5 dB by employing 2 μm fiber components and optimizing the microwire coupling losses.

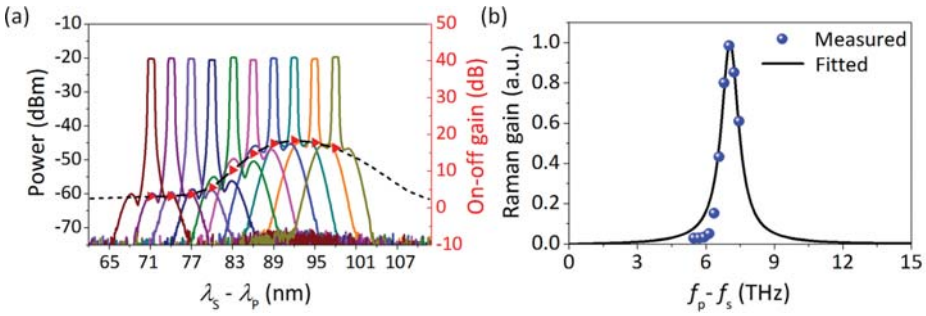

FIG. 3. (a) Measured Raman amplification spectra and extracted Raman gain as a function of probe wavelength λ_s shift with respect to pump wavelength $\lambda_p = 1.938\ \mu$m. The inferred Raman gain is presented by red triangles with right hand side vertical axis. (b) Normalized Raman gain as a function of frequency shift and fitted curve with a Lorentzian profile.

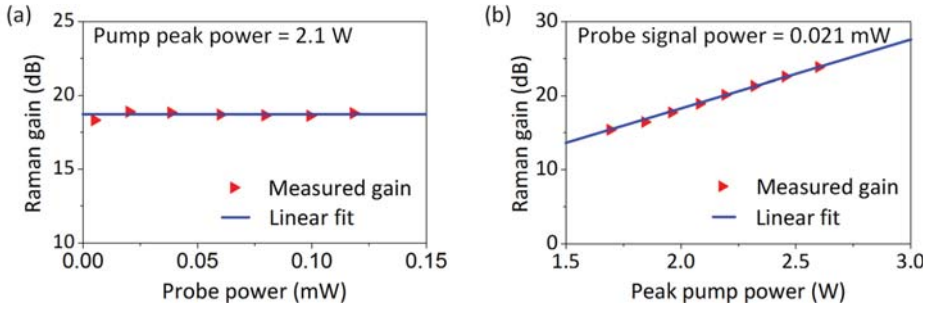

FIG. 4. (a) Measured Raman gain as a function of input probe power. (b) Measured Raman gain as a function of input peak pump power.

Laser oscillation is observed when the total Raman gain exceeds the total round-trip cavity loss and Raman pulses in the cavity are synchronized to the incoming pump pulses. Figure 6(a) shows the evolution of the laser output spectrum as the pump power is increased. The inset shows the average output power as a function of average pump power. The laser threshold is reached at an average pump power of 1.69 mW, corresponding to a peak power of 4.6 W, with a slope efficiency of 4.5%. The slope efficiency could be further improved by a lower round-trip cavity loss and a higher output coupling ratio.

As the pump power is increased, the Raman laser bandwidth exceeds the Raman gain bandwidth of $As_{38}Se_{62}$ and shows flat-top spectral characteristics often seen in normal dispersion Raman fiber lasers.[6] The wide spectrum of the Raman laser possibly comes from two sources: one is that the spectrally broadened pump gives rise to a broadened Raman gain bandwidth; and the other source is that the pump interacts with Raman signal via cross-phase modulation. Such a spectrally wide Raman laser output can potentially be externally compressed to femtosecond pulses.

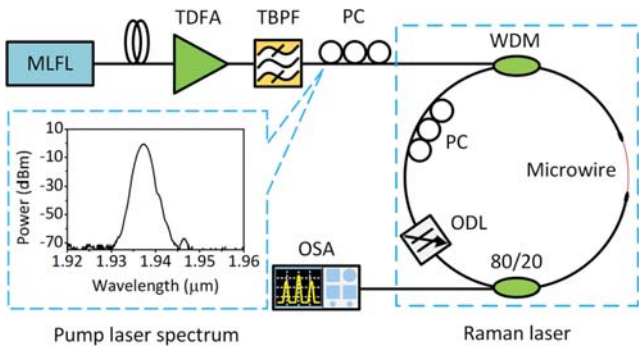

FIG. 5. Raman fiber laser experimental setup. MLFL: mode-locked fiber laser; TDFA: thulium-doped fiber amplifier; TBPF: tunable bandpass filter; WDM: wavelength division multiplexing coupler; PC: polarization controller; ODL: optical delay line; and OSA: optical spectrum analyzer.

The output wavelength of the Raman laser is tuned by adjusting the intra-cavity delay line and as a result of time-dispersion tuning. Figure 6(b) shows the output spectrum of the Raman laser at different cavity detuning values. The range of wavelength tunability is 8 nm, falling within the limits of Raman gain bandwidth.

To better understand the properties of the Raman fiber laser, numerical simulations are performed by solving the nonlinear Schrödinger equation (NLSE) using the split-step Fourier method.[26] The Raman response function derived above is incorporated in the NLSE for the multimaterial fiber and the microwire, while Raman scattering in silica fibers is ignored due to low peak power levels involved. Raman oscillation self-starts and reaches steady-state after a number of round-trips into which only the pump signal is injected into the resonant cavity. The circulating optical field containing both the Raman signal and the residual pump is filtered by the WDM coupler at the end of each round-trip. The Raman signal is delayed by 6.6 ps for synchronization before it is combined with a new pump pulse and fed back into the next round-trip. The Raman pulse energy and pulse width are monitored as a function of the number of round-trips to ensure that the numerical solution converges to a consistent solution. Figure 7(a) shows output spectra of the Raman fiber laser as a function of pump power, in good agreement with experimental results. As the peak pump power is increased, the Raman signal spectrum gradually develops a flat-top structure. Wavelength tunability is also confirmed by changing the temporal delay. Figure 7(b) shows output Raman pulses obtained by filtering and inverse Fourier transformation. Inspection of the phase content of the pulses reveals a strong linear chirp that can be compressed by applying a linear dispersion. Figure 7(c) shows the Raman pulses after recompression. As the peak pump power is increased, the compressed Raman pulse width decreases. However, due to the increased nonlinear chirp in the Raman pulses, compressed pulses exhibit increasingly prominent pedestals.

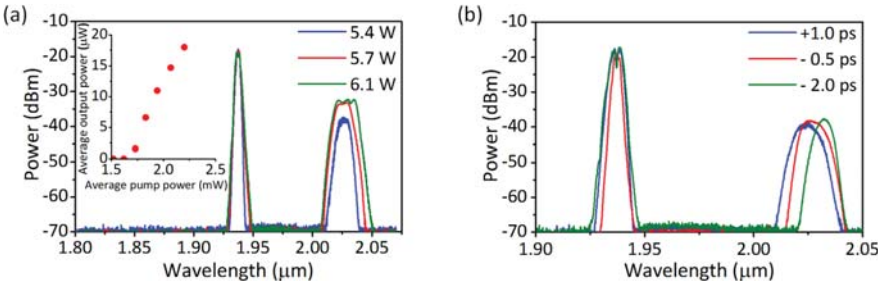

FIG. 6. (a) Output spectrum of the Raman laser with increasing pump power. Inset: Average output power versus average pump power. (b) Raman laser output spectrum at different relative cavity detuning values.

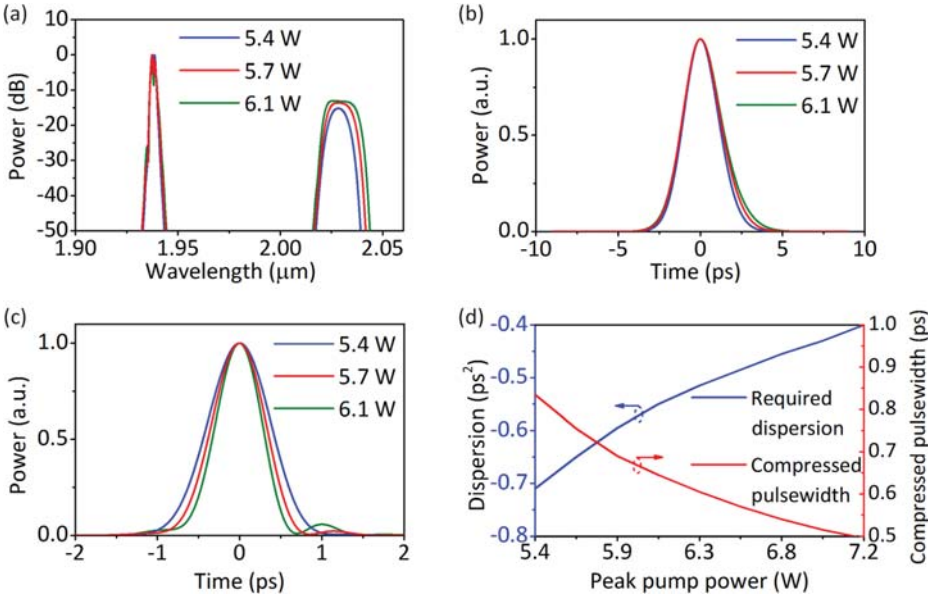

FIG. 7. (a) Simulated output spectra of the Raman fiber laser. (b) Simulated temporal shape of output Raman pulses and (c) after compression. (d) Required dispersion for optimal pulse compression and compressed pulse width as a function of peak pump power.

Figure 7(d) shows the amount of dispersion required for optimal compression and compressed pulse width as a function of peak pump power. In light of the simulations, output Raman pulses could be compressed to femtosecond pulses by propagating through, e.g., a few meters of fiber with anomalous dispersion.

In summary, we have demonstrated the operation of a Raman fiber laser based on a multimaterial chalcogenide microwire. The Raman laser emits at 2.025 μm from pump pulses centered at a wavelength of 1.938 μm. The threshold peak pump power of the Raman laser is 4.6 W, with a slope efficiency of 4.5%, which could be further improved by reducing the round-trip cavity loss and optimizing the output coupling ratio. The reach of laser output wavelength could be significantly extended towards longer wavelengths by enabling the operation of the second or higher order Raman shift.[27] Numerical simulation results are in good agreement with experimental observations, providing important insight into output Raman pulse evolution. Output Raman pulses can be compressed to femtosecond pulses by applying linear dispersion. The transmission window of the microwire is only limited by the transmission windows of $As_{38}Se_{62}$ and $As_{38}S_{62}$, which spans over the 1.5–11.0 μm wavelength range. This microwire is thus a promising gain medium for the fabrication of mid-infrared sources that are compact and operate with low-power consumption.

This work was financially supported by the Collaborative Research and Development Grants Program of the Natural Sciences and Engineering Research Council of Canada (NSERC).

[1]G. P. Agrawal, *Applications of Nonlinear Fiber Optics*, 2nd ed. (Academic Press, 2010).
[2]E. M. Dianov, M. Evgeny, and A. M. Prokhorov, IEEE J. Sel. Top. Quantum Electron. **6**, 1022 (2000).
[3]Y. Feng, L. R. Taylor, and D. B. Calia, Opt. Express **17**, 23678 (2009).
[4]F. Anquez, E. Courtade, A. Sivúry, P. Suret, and S. Randoux, Opt. Express **18**, 22928 (2010).
[5]D. S. Kharenko, A. E. Bednyakova, E. V. Podivilov, M. P. Fedoruk, A. Apolonski, and S. A. Babin, Opt. Lett. **41**, 175 (2016).
[6]D. Churin, J. Olson, R. A. Norwood, N. Peyghambarian, and K. Kieu, Opt. Lett. **40**, 2529 (2015).
[7]C. E. Castellani, E. J. Kelleher, J. C. Travers, D. Popa, T. Hasan, Z. Sun, E. Flahaut, A. C. Ferrari, S. V. Popov, and J. R. Taylor, Opt. Lett. **36**, 3996 (2011).
[8]E. M. Dianov, I. A. Bufetov, V. M. Mashinsky, A. V. Shubin, O. I. Medvedkov, A. E. E. Rakitin, M. A. Mel'kumov, V. F. Khopin, and A. N. Gur'yanov, Quantum Electron. **35**, 435 (2005).
[9]R. E. Slusher, G. Lenz, J. Hodelin, J. Sanghera, L. B. Shaw, and I. D. Aggarwal, J. Opt. Soc. Am. B **21**, 1146 (2004).
[10]O. P. Kulkarni, C. Xia, D. J. Lee, M. Kumar, A. Kuditcher, M. N. Islam, F. L. Terry, M. J. Freeman, B. G. Aitken, S. C. Currie, and J. E. McCarthy, Opt. Express **14**, 7924 (2006).
[11]V. S. Shiryaev and M. F. Churbanov, J. Non-Cryst. Solids **377**, 225 (2013).
[12]M. Bernier, V. Fortin, M. El-Amraoui, Y. Messaddeq, and R. Vallée, Opt. Lett. **39**, 2052 (2014).
[13]R. Ahmad and M. Rochette, Appl. Phys. Lett. **101**, 101110 (2012).
[14]S. D. Jackson and G. Anzueto-Sanchez, Appl. Phys. Lett. **88**, 221106 (2006).
[15]M. Bernier, V. Fortin, N. Caron, M. El-Amraoui, Y. Messaddeq, and R. Vallée, Opt. Lett. **38**, 127 (2013).
[16]P. Dumais, A. Villeneuve, P. G. J. Wigley, F. Gonthier, S. Lacroix, G. I. Stegeman, and J. Bures, Opt. Lett. **18**, 1996 (1993).
[17]E. C. Mägi, L. B. Fu, H. C. Nguyen, M. R. Lamont, D. I. Yeom, and B. J. Eggleton, Opt. Express **15**, 10324 (2007).

[18]C. Baker and M. Rochette, Opt. Express **18**, 12391 (2010).
[19]C. Baker and M. Rochette, Opt. Mater. Express **1**, 1065 (2011).
[20]L. Li, A. Al-Kadry, N. Abdukerim, and M. Rochette, Opt. Mater. Express **6**, 912 (2016).
[21]S. Shabahang, G. M. Tao, J. J. Kaufman, and A. F. Abouraddy, J. Opt. Soc. Am. B **30**, 2498 (2013).
[22]L. Vácha, M. Granberg, P. Marcollà, and U. Lindborg, J. Non-Cryst. Solids **38**, 797 (1980).
[23]G. Xue, B. Zhang, K. Yin, W. Yang, and J. Hou, Opt. Express **22**, 25976 (2014).
[24]R. H. Stolen, J. P. Gordon, W. J. Tomlinson, and H. A. Haus, J. Opt. Soc. Am. B **6**, 1159 (1989).
[25]G. Lenz, J. Zimmermann, T. Katsufuji, M. E. Lines, H. Y. Hwang, J. S. Sanghera, and I. D. Aggarwal, Opt. Lett. **25**, 254 (2000).
[26]G. P. Agrawal, *Nonlinear Fiber Optics*, 5th ed. (Academic Press, New York, 2013).
[27]F. Vanier, Y. A. Peter, and M. Rochette, Opt. Express **22**, 28731 (2014).